Technical Notes

Influence of Boundary Conditions on Stability of Thin-Walled Cylindrical Shells under Axial Load and Internal Pressure

GÜNTER FISCHER*
Institut für Festigkeit der Deutschen Versuchsanstalt für Luft- und Raumfahrt E.V., Mülheim Ruhr, Germany

Nomenclature

R, L, t	= radius of cylinder, length, thickness of wall
λ	= $L[3(1-\nu^2)]^{1/4}/Rt$
E, ν	= Young's modulus, Poisson's ratio
D	= $Et^3/12(1-\nu^2)$
$\varkappa$	= $16\pi^2[3(1-\nu^2)]^{1/2}R/t$
$x,\xi = x/2\pi R$	= coordinates
$y,\eta = y/2\pi R$	= coordinates
N	= axial load $[kp/cm]$
$\bar{N}$	= $[3(1-\nu^2)]^{1/2}NR/Et^2$
$\bar{N}_{cr}$	= critical axial load
$\bar{N}_{cr\ min}$	= minimum critical load
$\bar{N}_{cl}$	= classical load
p	= internal pressure
$\bar{p}$	= $[3(1-\nu^2)]^{1/2}pR^2/Et^2$
n	= number of waves in circumferential direction
λ_n	= $\varkappa/2(2\pi n)^2$
M	= differential operator
w, ω, f_0, f_n	= radial buckling displacements $\omega=(Et/D)^{1/2}\cdot w$
$\phi, \bar{\phi}, g_0, g_n$	= stress functions $\bar{\phi}=\phi/D+\eta^2\varkappa\bar{N}/2+\xi^2\varkappa\nu\bar{N}/2$
$A, \tilde{A}, B, \tilde{B}, \tilde{W}_1, \tilde{W}_2$	= quadratic matrices

Introduction

At the Gesellschaft für Angewandte Mathematik und Mechanik (GAMM) meeting in April 1962, the author[1] reported for the first time on the dependence of buckling loads of thin-walled cylindrical shells on boundary conditions that hitherto had been neglected. The critical axial loads for a simply supported shell found in theory corresponded well to the results concerning higher internal pressure that had been obtained by experiment. The correspondence was not as good for low internal pressure because, in that case, the influence of initial deformations is considerable, and the test cylinders produced hitherto differed largely from the ideal form.

Since the shells produced by industry are normally imperfect, the theory of the ideal shells could not be of any practical use. Therefore, at first we did not intend to make any further investigations as to the results already published in Ref. 2. Instead we started with investigations on the buckling loads of imperfect shells.

In October 1962, Stein[3] reported about his work on buckling loads of imperfect shells at the NASA Symposium on Instability of Shell Structures. He had gained very different results for other boundary conditions. During 1963, the theoretical buckling loads given in Refs. 1 and 2 were confirmed by a series of experimental works (e.g., Refs. 4–7), which had succeeded in producing nearly perfect shells. This is the reason for resuming the calculation and for studying the condition of clamped edges and the influence of parameters, too.

Received July 16, 1964; revision received December 22, 1964.
* Head, Strength and Dynamics Section.

Analysis

The deduction of the eigenvalue equation for a shell with clamped edges is in absolute analogy to Ref. 2. The large-deflection state of a shell is described by Maguerre's basic differential equations

$$D\Delta\Delta w = \frac{\partial^2\phi}{\partial y^2}\frac{\partial^2 w}{\partial x^2} + \frac{\partial^2\phi}{\partial x^2}\frac{\partial^2 w}{\partial y^2} - 2\frac{\partial^2\phi}{\partial x\partial y}\frac{\partial^2 w}{\partial x\partial y} + \frac{1}{R}\frac{\partial^2\phi}{\partial x^2} - p \tag{1}$$

$$\frac{1}{Et}\Delta\Delta\phi = \left(\frac{\partial^2 w}{\partial x\partial y}\right)^2 - \frac{\partial^2 w}{\partial x^2}\frac{\partial^2 w}{\partial y^2} - \frac{1}{R}\frac{\partial^2 w}{\partial x^2}$$

The boundary conditions for an axially loaded cylindrical shell with clamped edges and prevented radial edge-displacements are

$$w = 0 \qquad \partial w/\partial x = 0$$
$$\partial^2\phi/\partial x^2 = -\nu N \qquad \partial^2\phi/\partial y^2 = -N \tag{2}$$

The nondimensional solution ω of the given boundary-value problem for the prebuckling state is the known axisymmetric form

$$\omega = f_0(\xi) = -2(\nu\bar{N}+\bar{p})\times \{1 + C_1\cosh\tfrac{1}{2}[\varkappa(1-\bar{N})]^{1/2}\xi\cdot\cos\tfrac{1}{2}[\varkappa(1+\bar{N})]^{1/2}\xi + C_2\sinh\tfrac{1}{2}[\varkappa(1-\bar{N})]^{1/2}\xi\cdot\sin\tfrac{1}{2}[\varkappa(1+\bar{N})]^{1/2}\xi\} \tag{3}$$

with the integration constants

$$C_1 = -\frac{(1-\bar{N})^{1/2}\cosh a_1\sin a_2 + (1+\bar{N})^{1/2}\sinh a_1\cos a_2}{(1-\bar{N})^{1/2}\cos a_2\sin a_2 + (1+\bar{N})^{1/2}\sinh a_1\cosh a_1} \tag{4}$$

$$C_2 = \frac{(1-\bar{N})^{1/2}\sinh a_1\cos a_2 - (1+\bar{N})^{1/2}\cosh a_1\sin a_2}{(1-\bar{N})^{1/2}\sin a_2\cos a_2 + (1+\bar{N})^{1/2}\cosh a_1\sin a_1}$$

where a_1 and a_2 are

$$a_1 = \tfrac{1}{2}[\varkappa(1-\bar{N})]^{1/2}(L/4\pi R)$$
$$a_2 = \tfrac{1}{2}[\varkappa(1+\bar{N})]^{1/2}(L/(4\pi R)$$

In order to get the buckling load we have to introduce

$$\omega(\xi,\eta) = f_0(\xi) + f_n(2\pi n\xi)\cdot\cos 2\pi n\eta$$
$$\bar{\phi}(\xi,\eta) = g_0(\xi) + g_n(2\pi n\xi)\cdot\cos 2\pi n\eta \tag{5}$$

into the basic equations. Assuming the functions f_n and g_n to be small and neglecting the terms of the second order, we obtain the homogeneous system

$$M[f_n] = f_n^{IV} - 2f_n'' + f_n = \lambda_n[-(2/\varkappa)(\partial^2 f_0/\partial\xi^2)g_n + f_0 f_n + g_n'' - 2\bar{N}(f_n'' - \nu f_n)] \tag{6}$$

$$M[g_n] = g_n^{IV} - 2g_n'' + g_n = \lambda_n[(2/\varkappa)(\partial^2 f_0/\partial\xi^2)f_n - f_n''] \hat{=} \partial/\partial 2\pi n\xi$$

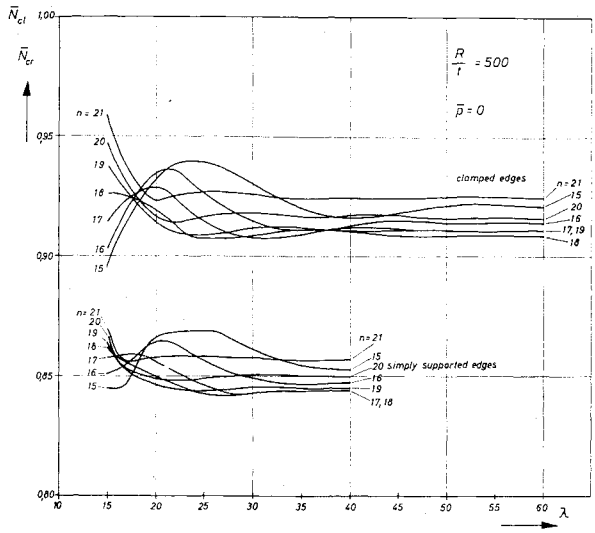

Fig. 1 Buckling loads $\bar{N}_{cr}$ vs cylinder length λ.

The homogeneous boundary conditions (the inhomogeneous boundary conditions (2) are satisfied by the axisymmetrical form) are

$$f_n = 0 \qquad f_n' = 0$$
$$g_n = 0 \qquad g_n'' = 0 \tag{7}$$

This eigenvalue [Eqs. (6) and (7)] problem is solved by a finite difference method. By means of finite forms, the system of differential equations may be converted into a system of algebraic equations, the coefficient determinant of which has to be zero:

$$\det[\tilde{A} + 2\bar{N}\tilde{B} - \tilde{W}_1 + (B - \tilde{W}_2)A^{-1}(\tilde{B} - \tilde{W}_2)] = 0 \tag{8}$$

The numerical solution of the eigenvalue problem was computed on an IBM 1620.

Discussion

The nondimensional, homogeneous, differential equations, Eq. (6), contain the following three parameters, the influence of which on the buckling loads shall be investigated as follows: In the nonconstant coefficients, which are f_0, $(1/\varkappa)(\partial^2 f_0/\partial\xi^2)$, respectively, according to Eqs. (3) and (4), 1) the nondimensional length $\lambda = L[3(1 - \nu^2)]^{1/4}/Rt$ in the integration constants C_1 and C_2; 2) the quotient R/t in the arguments of the trigonometric functions; and 3) on the right sides of the system (6), the factor $\lambda_n \sim R/tn^2$.

In Fig. 1 the critical loads $\bar{N}_{cr}$ of a clamped and a simply supported cylinder are plotted vs nondimensional length λ for

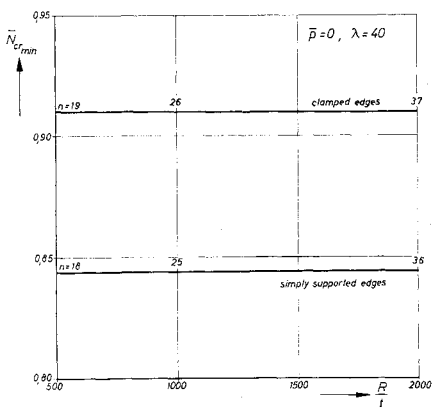

Fig. 2 Minimum buckling loads $\bar{N}_{cr_{min}}$ vs ratio R/t.

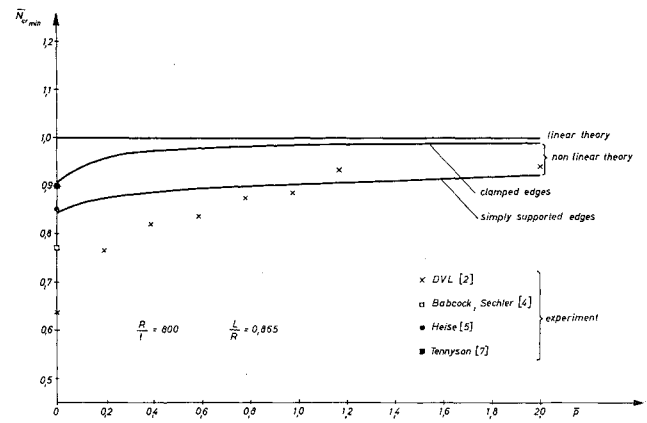

Fig. 3 Comparison between minimum buckling loads $\bar{N}_{cr_{min}}$ vs internal pressure $\bar{p}$ and experiment.

different wave numbers and const $R/t = 500$. For very short cylinders the dependence of $\bar{N}_{cr}(n)$ on length is the greatest. From a certain length λ_0, the $\bar{N}_{cr}(n)$ are independent from λ, as the axisymmetrical deformations caused by the prevented edge-displacement fade from the edge and cannot influence each other any longer. This value λ_0 can be easily estimated as follows. The factor $\bar{D}$ expressing the damping of the axisymmetric deformation f_0 is

$$\bar{D}(\xi) = e^{1/2[\varkappa(1-\bar{N})]^{1/2}(\xi-\xi_R)}$$

with

$$\xi_R = L/4\pi R$$

In the middle line of the cylinder ($\xi = 0$) this factor is

$$\bar{D}(0) = e^{-1/2\lambda(1-\bar{N})^{1/2}}$$

If we insert, for the clamped and simply supported cylinders, the median critical load $\bar{N}_{cr} = 0.92$ and $\bar{N}_{cr} = 0.85$, respectively, and suppose the influence of the edge nearly disappears (as soon as $\bar{D}$ is $\frac{1}{1000}$ of its edge-value), we obtain

$$\lambda_0 \approx 50 \qquad \lambda_0 \approx 35$$

in adequate correspondence with the results given in Fig. 1. It is also found that, in contrast to the buckling loads $\bar{N}_{cr}$, the minimum critical load $\bar{N}_{cr_{min}}$ for the lengths of cylinders $\lambda > 20$ is practically independent from λ.

Figure 2 shows the dependence of the minimum critical load $\bar{N}_{cr_{min}}$ from the quotient R/t. For λ_n, a nearly constant value for the whole interval results, i.e., R/t growing enlarges the number of circumference waves. Figure 3 is a supplement to Fig. 9 of Ref. 2. For various internal pressures, the minimum critical buckling loads $\bar{N}_{cr_{min}}$ for a cylinder ($R/t = 800$, $L/R = 0.865$) with clamped and simply supported edges were computed. As these buckling loads $\bar{N}_{cr_{min}}$ are nearly independent from the geometrical parameters $\lambda(\lambda > 20)$ and R/t shown in Figs. 1 and 2, these results are valid for cylinders with different geometrical dates, too. Last year's test results are plotted in Fig. 3.

References

[1] Fischer, G., "Über die Berechnung der kritischen Axiallasten gelenkig gelagerter Kreiszylinderschalen mit Hilfe des Mehrstellenverfahrens," Z. Angew. Math. Mech. **42** (1962).

[2] Fischer, G., "Über den Einfluss der gelenkigen Lagerung auf die Stabilität dünnwandiger Kreiszylinderschalen unter Axiallast und Innendruck," ZFW **11** (March 1963).

[3] Stein, M., "The effect on the buckling of perfect cylinders of prebuckling deformations and stresses induced by edge support," NASA TN D-1510 (1962).

[4] Babcock, C. D. and Sechler, E. E., "The effect of initial imperfections on the buckling stress of cylindrical shells," NASA TN D-2005 (1963).

[5] Heise, O., "Die experimentelle Ermittlung der Beullasten von längsgedrückten dünnwandigen Kreiszylinderschalen," Deut. Ber. Forschungsanstalt Luftfahrt 214 (1963).

[6] Almroth, B. O., Holmes, A. M. C., and Brush, D. O., "An experimental study of the buckling of cylinders under axial compression," Lockheed Missiles and Space Co. Rept. LMSC 6-90-63-104 (1963).

[7] Tennyson, R. C., "A note on the classical buckling load of circular cylindrical shells under axial compression," AIAA J. 1, 475–476 (1963).

Normal Spectral Emissivity of Isotropic and Anisotropic Materials

G. W. Autio* and E. Scala†
Cornell University, Ithaca, N. Y.

THE effects of crystallographic orientation, at or near the surface, upon the emission of radiant energy have not been sufficiently studied. The current investigation is being made on a number of isotropic and anisotropic materials. The results for high-purity single crystal nickel and pyrolytic graphite are discussed herein. The high anisotropy of pyrolytic graphite allows one to readily examine the orientation effect upon $\epsilon_{n\lambda}$, the normal spectral emissivity. The "ity" ending is used because the specimen surfaces are highly polished and the materials are of excellent purity and soundness. The available literature indicates that very little investigation has been made of the normal spectral emissivity of single crystal nickel, pyrolytic graphite, and polycrystalline graphite in the near infrared region of the electromagnetic spectrum.

A schematic of the experimental apparatus employed is shown in Fig. 1. Four specimens can be embedded in the top of a high-purity and dense graphite block with good thermal contact. The blackbody cavity is a drilled hole in this graphite block of depth to diameter ratio of 6.75. Any one of the specimens or the blackbody cavity can be aligned with the water-cooled sight tube by rotating the control rod. Measurements are made sequentially by pulling up the graphite block to within about 0.050 in. from the end of the sight tube. That is, after each reading of a specimen or the blackbody, the graphite block is lowered to the uniform hot zone. The radiant energy is focused into the monochromator entrance slits by means of a spherical and a plane mirror. The same optical path is used for all specimens and the blackbody cavity.

With the specimen in the down position, at equilibrium temperature, the recorded millivolt level represents reflected and extraneous radiation as well as that emitted by the specimen. As the specimen is drawn up to the sight tube, a sharp decrease is recorded, until the radiant energy emitted by the specimen alone is obtained. The trace is linear between these points for about 3 sec, after which the slope deviates from linearity, representing the cooling of the specimen. The possible error due to radiant energy from the furnace tube walls is kept to a minimum by maintaining the smallest gap feasible without contact. Since the blackbody cavity reflects essentially no radiation, the change in its millivolt level is small (<0.10 mv) compared to a specimen (>1.0 mv) as the cavity is drawn up to the sight tube. The normal spectral emissivity of the specimen is the ratio of the millivolt reading of the specimen to that of the blackbody cavity for the same wavelength setting on the monochromator drum.

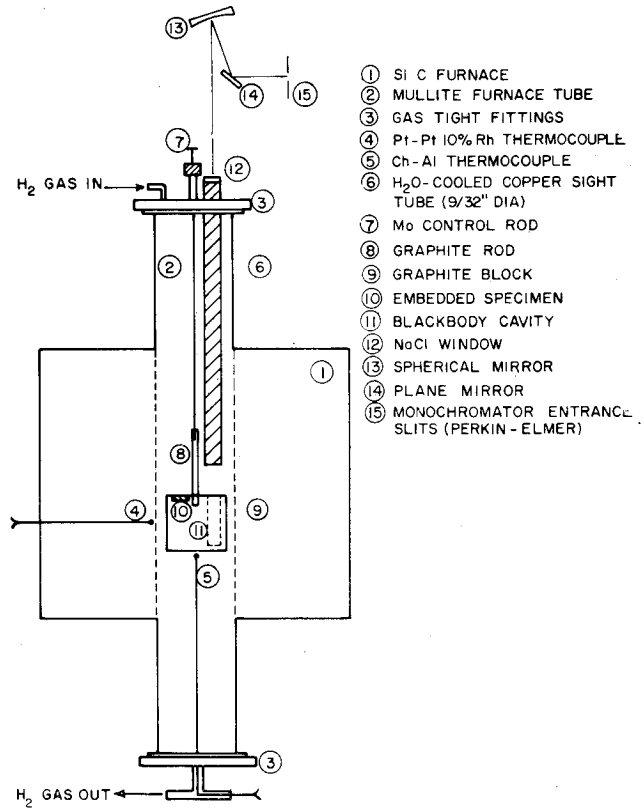

Fig. 1 Furnace schematic.

This technique has four desirable features: 1) the blackbody cavity and all specimens are as one unit under the same heating conditions; 2) the same optical path is used for the blackbody cavity and all specimens; 3) the measurements are strictly relative to the well-defined blackbody cavity; and 4) the optics employed are relatively simple. Whereas other techniques[1] may permit smaller errors of absolute measurement of emissivity, the method employed here allows for excellent comparative measurements on specimens of different crystallographic orientation. Normal spectral emissivity data for polycrystalline and single crystal nickel, pyrolytic graphite, and polycrystalline graphite are compared in Figs. 2–4. Data for these and other materials at temperatures down to 800°C have also been obtained.

The pyrolytic graphite is a Supertemp material formed at about 2150° C to a thickness of about 0.375 in. The polycrystalline nickel is the high-purity 270 grade (Huntington Alloy Products Division). The single crystal nickel (0.750-in. diam) was grown from the 270 grade by B. F. Addis in J. L. Gregg's Crystal Growing Laboratory at Cornell University. The measurements were performed in a hydrogen atmosphere to prevent any surface changes due to oxidation and the anomalous surface effects observed in vacuum or "neutral" gases. Photomicrographs (up to 1000×), interference photographs and x ray, back-reflection, and transmission Laue patterns were taken of all the specimens before and after the experiments to check the orientations and surface changes. In the results reported here, the specimens showed no evidence of orientation or surface changes.

The data on polycrystalline nickel compares favorably with the published results of Hurst,[2] Seban,[3] Ward,[4] Price,[5] and Reid[6] (Fig. 2). For polycrystalline nickel, there is agree-

Received August 13, 1964; revision received September 10, 1964. This technical note is part of a thesis to be submitted by G. W. Autio in partial fulfillment for the M. S. degree at Cornell. This research is supported by the Advanced Research Projects Agency.

* Research Assistant.
† Professor. Member AIAA.